JOURNAL OF MATERIALS SCIENCE 31 (1996) 4709–4718

Microstructural homogeneity improvement in Si_3N_4 by a powder coating method

C. M. WANG*
School of Materials, University of Leeds, Leeds LS2 9JT, UK

The efficiency of a powder coating technique has been quantitatively evaluated through a comparison of the densification behaviour, green compact and dense material microstructural homogeneity in terms of a "homogeneity dimension", and mechanical properties, using coated powders and mixed powders in the case of Si_3N_4 powder densified by hot-pressing with the liquid-forming additive system Al_2O_3–TiO_2–SiO_2. For coated powder, a significantly smaller value of the homogeneity dimension was obtained. The oxide phases became re-distributed during densification, with the aluminium-containing phase distributed on a finer scale, and the titanium-containing phase on a coarser scale, compared with the green body. Materials prepared by hot-pressing of coated powders showed a more homogeneous microstructure, higher bend strength and higher Weibull modulus, compared with materials prepared from mixed powders. There were no differences in fracture toughness and hardness between the two types of material.

1. Introduction

Pure Si_3N_4 cannot be fabricated into fully dense components using either standard metallurgical techniques or traditional ceramic sintering methods; one successful fabrication technique was found to be liquid-phase sintering using a metal silicon oxynitride-based liquid. For this purpose, it is necessary to add small amounts of metal oxides, which at sintering temperature react with the natural surface, SiO_2, on the Si_3N_4 powder particles and with the Si_3N_4 itself to form a liquid. The liquid phase assists particle rearrangement and acts as a high diffusivity pathway for the subsequent solution–diffusion–precipitation process.

Traditionally, the mixing of two or more powders is achieved by ball milling or attrition milling. Firstly, the effectiveness of these means is limited by the initial particle size and size distribution; secondly, mass segregation may occur by sedimentation during the drying up process; thirdly, inevitably pick up of the milling medium components induces composition shift or causes contamination. Mass segregation may induce the formation of pore clusters or nests which are potentially strength degrading [1]. Inhomogeneous distribution of the sintering additive will also induce different compaction responses, and lead to green compact density inhomogeneity, which may, in turn, produce cracks and residual stress as a result of different shrinkage rates during densification [2].

A recent development in powder processing to achieve improved microstructural homogeneity is a colloidal powder doping process, termed "powder coating" [3–9]. Powder coating can be achieved typically through a sol–gel process [3, 8, 10–12], an *in situ* solution precipitation process [13–17], and a colloidal particles adsorption process [18–20], with each method having different limitations when applied to different powders. For silicon nitride powder coating with metal oxide, the solution precipitation method with metal alkoxide as precursors, there are some advantages in avoiding a water medium, thus preventing the surface oxidation of silicon nitride powders [5]. Although the powder coating process has been applied to different powders, and the effectiveness of powder coating has been qualitatively evaluated, mainly based on direct microstructural observation, quantitative evaluation of powder coating-related homogeneity improvement has not been reported.

The quantitative description of the degree of mixing in a two-component powder system has been addressed by Hupmann and Bauer [21] with the liquid-phase sintering of tungsten and copper. A degree of mixing parameter was experimentally determined, using the principles of quantitative metallography, quantitatively to describe the homogeneity of the mixed powder. It is difficult in practice to apply this method to much finer grain-size materials, and to the case of a solid solution, such as in β′-sialon.

An alternative approach to the quantitative description of the phase distribution uniformity in multiphase oxides ceramics has been developed by Lange and Hirlinger [22], based on SEM with energy dispersive X-ray analysis (EDS). When a multiphase body is observed by SEM, the X-rays collected produce an EDS spectrum that quantitatively defines the atomic fraction of each element. If different elements

Present address: National Institute for Research in Inorganic Materials, Naniki 1-1, Tsukuba-shi, Ibaraki 305, Japan.

0022–2461 © *1996 Chapman & Hall*

are associated with different phases, the content of each phase within the area scanned can be determined. At low magnifications, the EDS spectrum defines the fraction of each phase within the large body. With reasonable counting periods, the standard deviation for different areas examined at low magnification is low and associated with counting statistics. At very high magnifications, the area examined may not be representative of the large body. The scanned area may only cover one of the many phases, and the deviation of the spectrum, relative to the large body, can be very large. At some intermediate magnification, the standard deviation will begin to depart from that produced by counting statistics. At this magnification, the area scanned is statistically identical with the large body. The size of this area thus defines the smallest area that contains the same phase content ratio as the whole body. This area, A_u, can be defined quantitatively and used to represent the degree of phase homogeneity. A_u is an extrinsic property of multiphase materials that depend on the processing [23]. The more homogeneous the phase distribution, the smaller is A_u. However, the use of this quantitative method in evaluating the phase uniformity of non-oxides has not been reported.

The aim of this work was to evaluate the effectiveness of the powder coating technique, both qualitatively and quantitatively, through a comparison of powder densification behaviour, microstructural homogeneity in the state of the green compact and densified materials in terms of a "homogeneity dimension", and mechanical properties, using coated powders and mixed powders in the case of Si_3N_4 powder densified by hot pressing with the liquid-forming additive system Al_2O_3–TiO_2–SiO_2.

2. Experimental procedure

2.1. Powder processing and sample characterization

An optimized powder coating process was employed in the present experiment as described in detail elsewhere [5, 17]. Aluminium iso-propoxide ($Al[OCH(CH_3)_2]_3$) and titanium iso-butoxide ($Ti[(CH_3)_2CHCH_2O]_4$) (BDH Chemicals, Poole, UK) were dissolved in iso-propanol with a concentration of alkoxide: iso-propanol of 1:20 g cm^{-3}, and Si_3N_4 powder (Starck, LC12-N, Berlin, with a sedimentation mean particle size of 500 nm, nitrogen adsorption specific surface area of 17.4 m^{2}g^{-1}, initial α-silicon nitride content of 96%, and an oxygen content of 1.58 wt %), added to the solution. In order to improve the dispersion of Si_3N_4 powder, and the alkoxide adsorption on Si_3N_4 particle surfaces, the slurry was ball milled for 24 h. The slurry was then transferred to a flask under flowing nitrogen for controlled hydrolysis. A molar ratio of the total water to alkoxide of 20:1 was chosen to ensure complete hydrolysis of the alkoxide by deionized water diluted by iso-propanol to give a water concentration of 33% (by volume). Water was added dropwise (3 cm^3 min^{-1}) to the slurry at 22 °C. On completion of hydrolysis, the slurry was aged at room temperature in the mother liquid for 24 h to allow complete reaction and then dried under infrared radiation at 50 °C followed at 120 °C for 2 h to obtain a powder.

For mixed powders, commercial α-Al_2O_3 with an average particle size of 500 nm and specific surface area of 6.7 m^{2}g^{-1} (Realox-XA-1000SG, Alcoa, USA), and TiO_2 with a specific surface area of 211 m^{2}g^{-1} (NP90.235, Tioxide, UK) were used. The oxides and Si_3N_4 powder were dispersed in iso-propanol with a concentration of 100 mg cm^{-3} and ball milled for 24 h in a polyethene bottle (110 mm diameter, 80 mm height) filled with cylindrical Si_3N_4 milling media (7 mm diameter, and 9 mm height), which had weight three times that of the powder. The iso-propanol was then evaporated on a hot plate under infrared radiation at 50 °C, and the powder was finally dried at 120 °C for 2 h.

Both powders were hot-pressed at 1700 °C, and 20 MPa for periods of 0.46, 1.6 and 5.4 ks. The shrinkage of the samples was continuously monitored by a transducer and the data were collected by computer. Prior to hot pressing, the coated powder was calcined in air at 500 °C for 2 h to allow the dehydration of the coating layer; in view of the possibility of the pick up of extra oxygen during calcination, the mixed powder was also calcined under identical conditions. Thus the only difference between the two powders was the additive incorporation process.

The phase composition of the products was analysed by X-ray diffraction (XRD) using powders prepared by crushing hot-pressed discs in a tungsten carbide-lined mill. As internal standard, 10 wt % ~200 μm silicon powder was used, with CuK_α radiation on a Phillips APD1750 automatic powder diffraction system. The sample was scanned for a 2θ of ~10°–80° with a scanning speed of 2θ 0.01 °s^{-1}. The relative contents of the α- and β-phases were determined by the method proposed by Gazzara and Messier [24, 25]

$$\alpha = (-0.443R_\alpha^2 + 1.443R_\alpha) \quad (1)$$

$$R_\alpha = \frac{I_{\alpha(2\,1\,0)}}{I_{\alpha(2\,1\,0)} + I_{\beta(2\,1\,0)}} \quad (2)$$

where $I_{\alpha(2\,1\,0)}$ and $I_{\beta(2\,1\,0)}$ are the integrated α- and β-phase (2 1 0) peak intensities.

The relative contents of TiN and Si_2N_2O were also estimated by the integrated peak intensity method [26]

$$w_i = \frac{I_i}{\sum I_i} \quad (3)$$

where w_i is the fraction weight of phase i, I_i is the integrated intensity of phase i; α-Si_3N_4(2 1 0), β-Si_3N_4(2 1 0), Si(1 1 1), TiN(2 0 0) and Si_2N_2O(2 0 0) peaks were used.

The lattice parameters of β′-sialon were calculated from the equation for a hexagonal cell

$$\frac{1}{d^2} = \frac{4}{3}\left(\frac{h^2 + hk + k^2}{a^2}\right) + \frac{l^2}{c^2} \quad (4)$$

where ($h\,k\,l$) are the Miller indices, d is the lattice planar distance and a and c are the hexagonal lattice parameters. The (2 1 0) and (1 0 1) peaks were used to calculate a and c; d was calculated using the Bragg equation with 2θ calibrated by the silicon (1 1 1) peak with a lattice parameter of 543.01 pm (JCPDS card 5-655). The sialon z-value used is the average of two values obtained from the a and c cell dimensions using the following equations [27]

$$a = 760.3 + 2.96\,z\,\text{pm} \quad (5)$$

$$c = 290.7 + 2.55\,z\,\text{pm} \quad (6)$$

The strength of the hot-pressed materials was determined by four-point bending. Hot-pressed rectangular pieces were cut to dimensions of $25 \times 5 \times 4\ \text{mm}^3$ with a diamond impregnated blade, followed by grinding. Tension surfaces and bevelled edges were polished to 1 μm. All strength measurements were carried out using an Instron Universal Testing Machine (Type 115 UK) with a cross head speed of $0.1\ \text{mm min}^{-1}$ for hot-pressed materials, and $0.5\ \text{mm min}^{-1}$ for green bodies. The strength distribution function was calculated according to the two-parameter Weibull function [28]

$$P_f = 1 - \exp\left[-\left(\frac{\sigma}{\sigma_0}\right)^m\right] \quad (7)$$

where σ is the strength, σ_0 is the characteristic strength, P_f is the failure probability, and m is the Weibull modulus. For a group of specimens N, P_f was calculated by the median ranking method [29]

$$P_f = \frac{(i - 0.3)}{(N + 0.4)} \quad (8)$$

The Vickers hardness, H_v, and fracture toughness values for the hot-pressed materials were measured by the indentation of polished surfaces with a load of 50 N. K_{Ic} values were calculated according to the equation [30]

$$K_{Ic} = 0.016\left(\frac{E}{H_v}\right)^{1/2}\left(\frac{P}{c_i^{3/2}}\right) \quad (9)$$

where E is Young's modulus, c_i is the average radial crack length measured from the centre of the impression and P is load.

TEM powder samples were prepared by a standard method through dispersing the powder in iso-propanol with a concentration of $\sim 0.1\ \text{mg cm}^{-3}$ by ultrasonic agitation for 10 min and doping on a carbon film-covered copper grid. For hot-pressed materials, a 2 mm thick disc was cut and hand ground on silicon carbide paper to 50 μm. The sample was argon ion-beam thinned (Gatan, Duo Mill, Model 600, USA) at 20°, 0.5 mA and 6 kV for ~16 h until perforation, and 1 h at 10°, 1 h at 6° scattering was continued. A ~5 nm carbon film was sputtered to prevent the surface charging. TEM samples were examined in a Jeol 200 CX TEM/STEM instrument, operating at 200 kV, with an attached Link EDS system for elemental analysis.

2.2. Quantitative analysis of microstructural homogeneity

Relative elemental concentrations were analysed using SEM with EDS as developed by Lange and Hirlinger [22]. Carbon-coated specimens and the detector were positioned to optimize SEM viewing, and the acquisition of X-ray spectra. The filament voltage was 20 kV and the sensitivity of the multichannel analyser was selected as 20 eV per channel. A 28 mm working distance was chosen, and the spot size was adjusted so that the counting rate was ~2500 counts s^{-1}. Spectra were acquired for a period of 100 s. The number of X-ray photons (counts) was integrated between 1.40 and 1.60 keV for $AlK_{\alpha 1}$, between 1.62 and 1.92 keV for $SiK_{\alpha 1}$ and between 4.36 and 4.66 KeV for TiK_{α}, to determine the corresponding integrated peak intensities for aluminium, silicon and titanium. The deviation of the fractional ratio of these integrated peak intensities Al/(Al + Si + Ti) and Ti/(Al + Si + Ti) from values obtained at low magnification, as a function of scanning area or magnification, were used to characterize the phase homogeneity. The samples were analysed from low magnification to high magnification; the scanned area, A_u, was related to the magnification, M, on the Camscan 4 SEM, by

$$A_u = \left(\frac{123\,200}{M}\right)^2 \mu\text{m}^2 \quad (10)$$

For a definite magnification, 15–20 spectra were obtained by random movement of the sample. The Al/(Al + Si + Ti) and Ti/(Al + Si + Ti) standard deviations normalized to their mean values were plotted as a function of magnification. The statistical counting error was estimated by repeated scans of the same area at low magnification giving a normalized deviation of 4.9% for a polished surface and of 5.3% for a green body.

3. Results

3.1. Homogeneity evaluation in the green state

The 3 wt % TiO_2 and 7 wt % Al_2O_3 sintering additive was incorporated into Si_3N_4 either by conventional ball milling (termed "mixed powder"), or by a powder particle coating technique (termed "coated powder"). The two powder morphologies are shown in Fig. 1. In the mixed powder, the distribution of the three components, Si_3N_4, Al_2O_3 and TiO_2 can be described as a mixing of individual particles, together with a certain amount of agglomeration. Even with an initial TiO_2 powder of a primary particle size of ~10 nm, an agglomeration of TiO_2 particles in ~400 nm can be seen. However, in the coated powder, every Si_3N_4 particle appears to have become attached to the nano-dimension oxide particles, and the overall distribution of sintering additive is homogeneous on the scale of a few Si_3N_4 particle dimensions.

Both the coated and the mixed powders were die-pressed at 50 MPa and then isostatically pressed at 200 MPa. The phase distribution was analysed using the SEM by EDS on the smooth, as-pressed, surfaces.

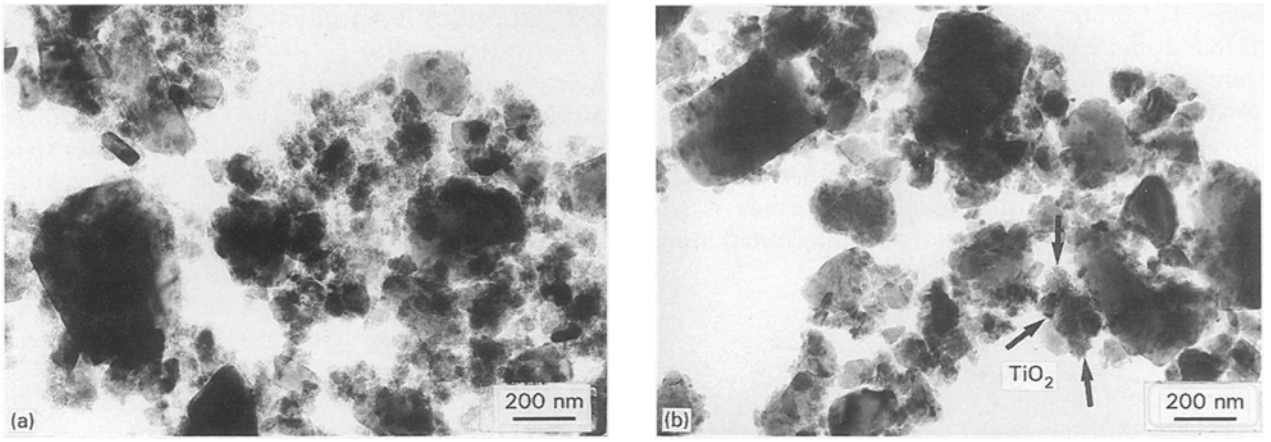

Figure 1 Transmission electron micrographs of Si_3N_4 powder containing 7% Al_2O_3 and 3% TiO_2, (a) coated, (b) mixed.

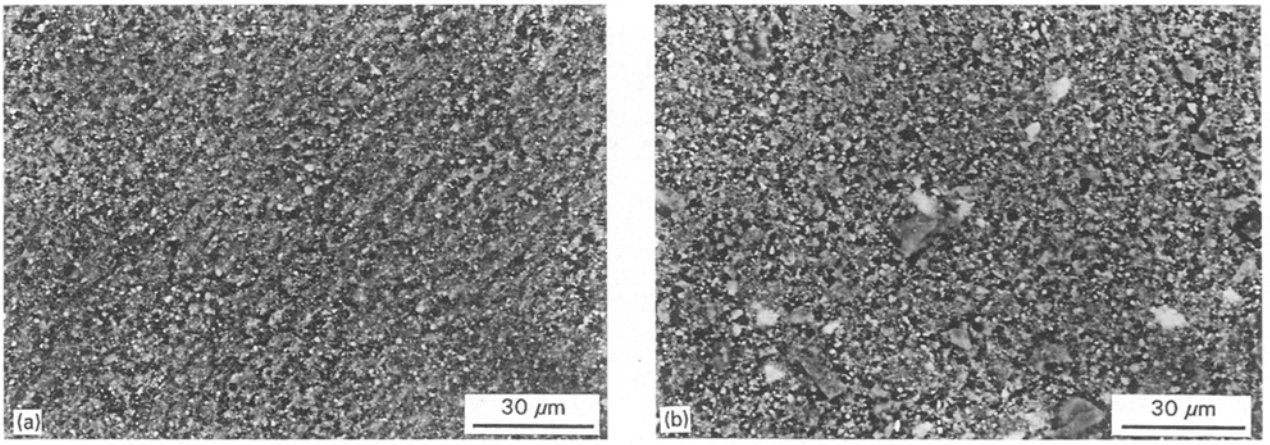

Figure 2 SEM back-scattered images in a green body showing the distribution of TiO_2 (a) coated, and (b) mixed.

Fig. 2 shows scanning electron micrographs in the back-scattered imaging mode. In the back-scattered electron images, the concentration of TiO_2 appears in an obvious light contrast, because of the higher atomic number of titanium. It is obvious that titanium containing species are more homogeneously distributed in the compact prepared from coated powder, than from mixed powder. Even taking into account the fact that the initial TiO_2 powder has a primary particle size of ~ 10 nm, and the Al_2O_3 500 nm, the mixed powder compact included agglomerates of TiO_2 as large as 4 μm, showing that primary particle size is not necessarily a key factor in achieving a higher degree of phase dispersibility.

Fig. 3 shows the standard deviations of Ti/(Si + Al + Ti) and Al/(Si + Al + Ti), each normalized by the mean value, as a function of microscope magnification factor. For both titanium and aluminium, the deviation gradually increases with increasing magnification (decreasing size of the analysed area). The smallest area that represents the mean overall phase distribution can therefore be calculated from Equation 10. A mean standard deviation of 5.3% is the statistical counting error for green bodies. Table I lists the phase distribution homogeneity dimension, which is also indicated in the number of Si_3N_4 particle mean dimensions (with a mean particle size of

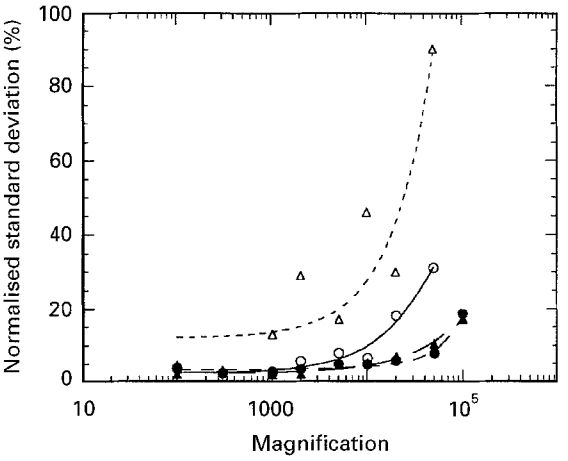

Figure 3 Normalized standard deviations of Al/(Al + Si + Ti) and Ti/(Al + Si + Ti) count ratios as a function of magnification in green compacts of Si_3N_4 containing 7% Al_2O_3 and 3% TiO_2. (--●--) Coated aluminium, (–○–) mixed aluminium, (–▲–) Coated titanium, (··· △ ···) mixed titanium.

~ 500 nm). For coated powder, aluminium has a homogeneity dimension of approximately 12 Si_3N_4 particle dimensions, and titanium approximately 14. For mixed powders, the aluminium homogeneity dimension is 40, and titanium is 240. Thus the

homogeneity dimension in the coated powder is reduced by a factor of 4 for aluminium and 20 for titanium, as compared with that of the mixed powder.

3.2. Densification, phase composition and properties

Density as a function of hot-pressing time is shown in Fig. 4. The coated powder densifies faster than the mixed powder, and reaches ~99% relative density in ~150 s, compared to ~250 s for the mixed powder.

X-ray phase analysis shows that both hot-pressed materials were composed of α-Si_3N_4, β′-Si_3N_4, TiN and Si_2N_2O. Normalized peak heights as a function of hot-pressing time are shown in Fig. 5. With increasing hot-pressing time, the Si_2N_2O, and β′-Si_3N_4 peaks increase, and that of α-Si_3N_4 decreases while that of TiN is constant after ~460 s. After hot-pressing for 460 s, 68% α-phase was detected in the coated powder, in contrast to 74% in the mixed powder, implying that the α- to β′-Si_3N_4 phase transformation is slightly faster in the coated powder than in the mixed powder during this short period of hot-pressing. Fig. 6 shows the proportion of α-phase as a function of time. The time exponents are $4.6 \times 10^{-4}\ s^{-1}$ and $4.8 \times 10^{-4}\ s^{-1}$ for coated and mixed powder, respectively. The β′-Si_3N_4 z-values are plotted as a function of hot-pressing time in Fig. 7. The z-values decrease with increasing hot-pressing time. At the beginning of densification, the amount of β-Si_3N_4 available for absorbing Al_2O_3 is less and hence gives a higher aluminium solute concentration in the β′-Si_3N_4 grains. With longer times, more β′-Si_3N_4 formed, and the aluminium solutes redistributed, giving lower z-values.

Fracture toughness and Vicker's hardness as a function of hot-pressing time are shown in Fig. 8. There are not significant differences between the two materials; fracture toughness increases and Vickers hardness decreases with increasing hot-pressing time. The mean four-point bend strengths of materials hot-pressed for 460 s are 310 MPa for coated powder material and 282 MPa for mixed powder material. There is a 10% improvement in the mean strength with the coated material, as shown in the strength distribution in Fig. 9. The Weibull modulus of a material produced from coated powder is 18, compared with 7 for material from the mixed powder.

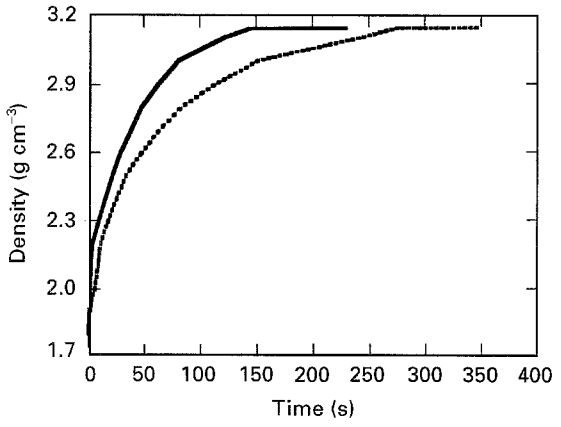

Figure 4 Density as a function of time during hot pressing at 1700 °C, 20 MPa: (··· ···) mixed, (—) coated.

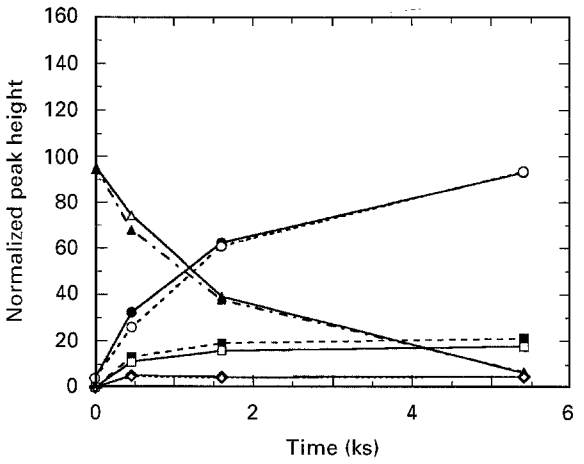

Figure 5 Normalized X-ray peak heights as a function of time after hot pressing at 1700 °C, 20 MPa. (▲, △) α-Si_3N_4, (●, ○) β-Si_3N_4, (◆, ◇) TiN, (■, □) Si_2N_2O; (▲, ●, ◆, ■) coated, (△, ○, ◇, □) mixed.

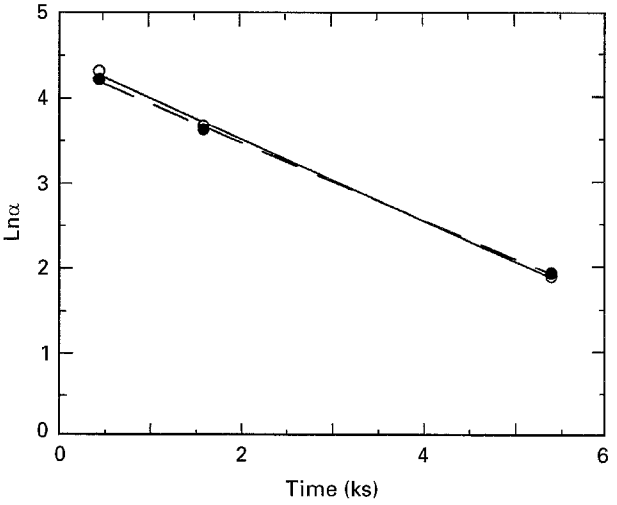

Figure 6 Logarithm of α-phase as a function of time after hot pressing at 1700 °C, 20 MPa. (–○–) mixed, $\alpha = 90.0 \exp(-4.8 \times 10^{-4} t)$, (–●–) coated, $\alpha = 81.5 \exp(-4.6 \times 10^{-4} t)$.

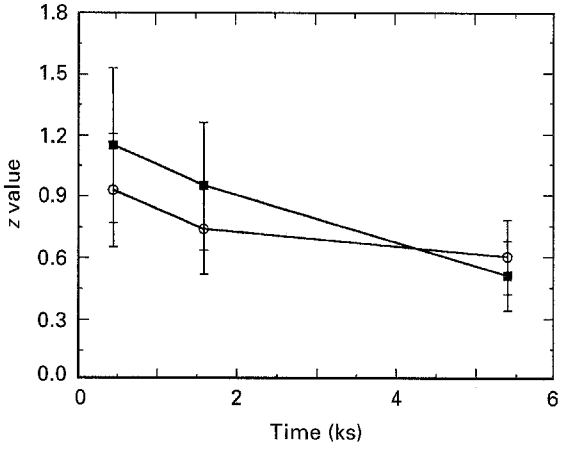

Figure 7 z-value as a function of time after hot pressing at 1700 °C and 20 MPa: (○) mixed, (■) coated.

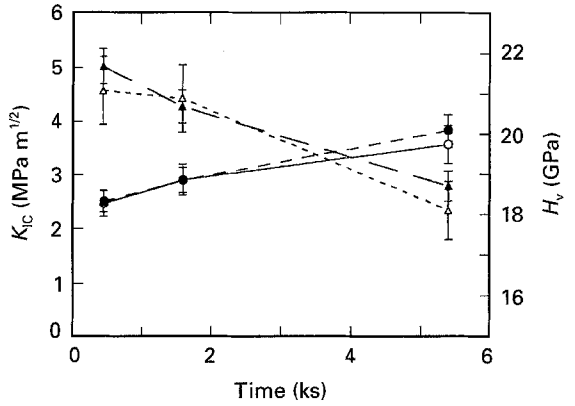

Figure 8 (●, ○) The fracture toughness, K_{Ic}, and (▲, △) hardness, H_v, as a function of time: (○, △) mixed, (●, ▲) coated.

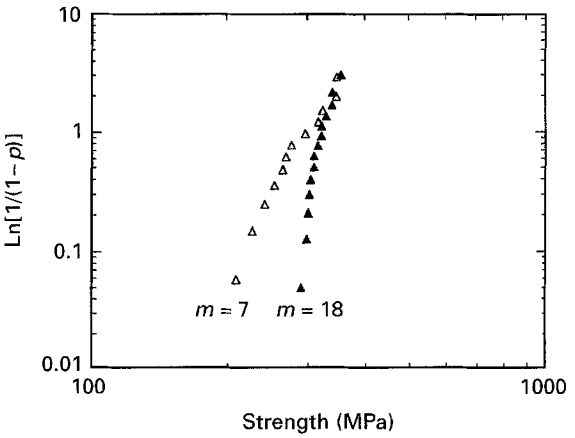

Figure 9 Weibull distribution of four-point bend strength for materials hot pressed at 1700 °C and 20 MPa for 460 s: (▲) coated, (△) mixed.

3.3. Homogeneity evaluation in densified materials

Polished and etched surfaces of 460 s hot-pressed materials are shown in Fig. 10. Both materials have a mean grain size of 1.0 μm. At larger scale observation, the mixed materials apparently include some heterogeneities which have a feature of pore-clustered structure with some as big as 5 μm after etching. Such a size of heterogeneity is not visible in the coated powder materials.

The transmission electron micrographs (Fig. 11) show that generally both materials are composed of fine-grain α-Si_3N_4, β′-Si_3N_4, TiN, Si_2N_2O. However, the distribution of TiN (which has a much darker contrast because of the large atomic number of titanium) in the Si_3N_4 matrix is dependent on the fabrication process. In the coated powder material, TiN particles with a size of 50–200 nm are homogeneously distributed. In the mixed powder material, TiN particles are distributed in the form of agglomerates, and in some areas, EDS shows high concentrations of both aluminium and titanium. Fig. 12 shows a typical phase distribution, with TiN in bright contrast in the back-scattered image. The distribution of titanium-containing phases is clearly more homogeneous in the coated powder material than in the mixed powder material. Some TiN agglomerates in the mixed powder material are as large as 5 μm, in contrast ~1 μm in the coated powder material.

Fig. 13 plots the normalized standard deviation of Ti/(Si + Ti + Al) and Al/(Si + Ti + Al) as a function of magnification. The smallest area that represents the mean phase distribution could therefore be calculated from Equation 10 with a mean deviation of 4.9% as the deviation due to the statistical counting error in the dense material; the homogeneity dimension for each phase is listed in Table I. In the mixed powder material, the aluminium containing phase has a homogeneity dimension of ~10 μm, and the titanium-containing phase one of ~120 μm. In the materials made from coated powder, the aluminium-containing phase has a homogeneity

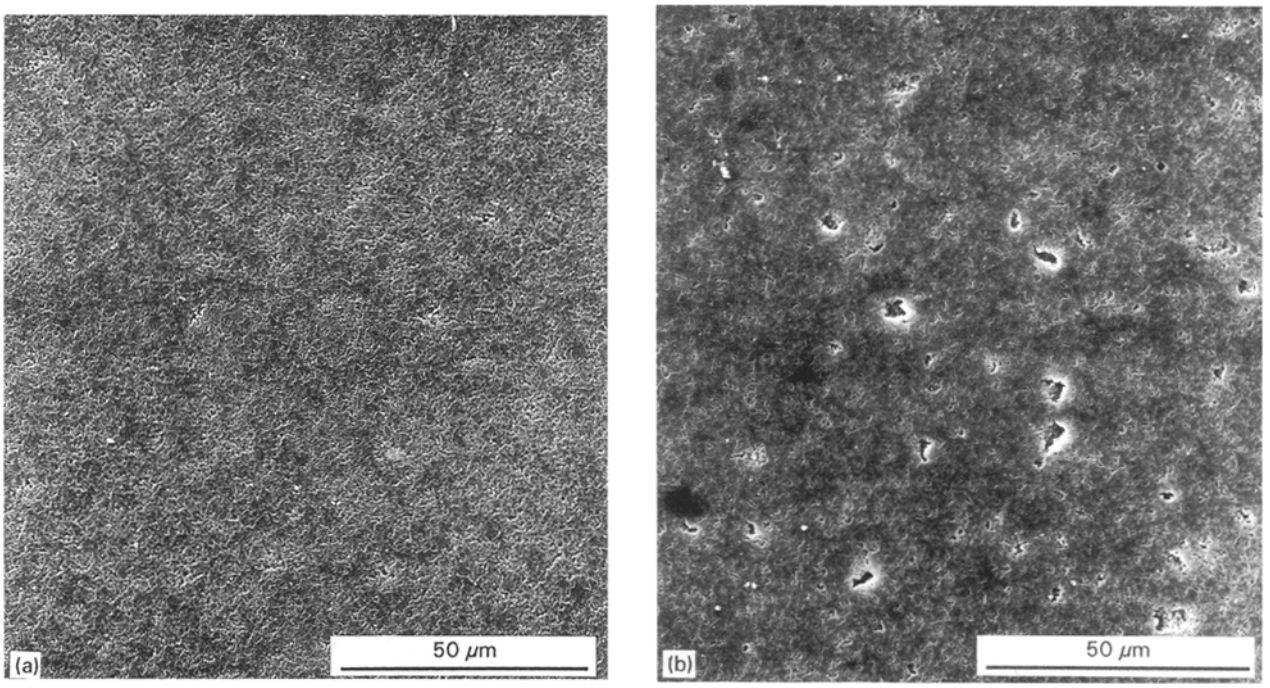

Figure 10 Scanning electron micrographs of polished and KOH etched surfaces of materials hot pressed at 1700 °C and 20 MPa for 460 s, (a) coated and (b) mixed.

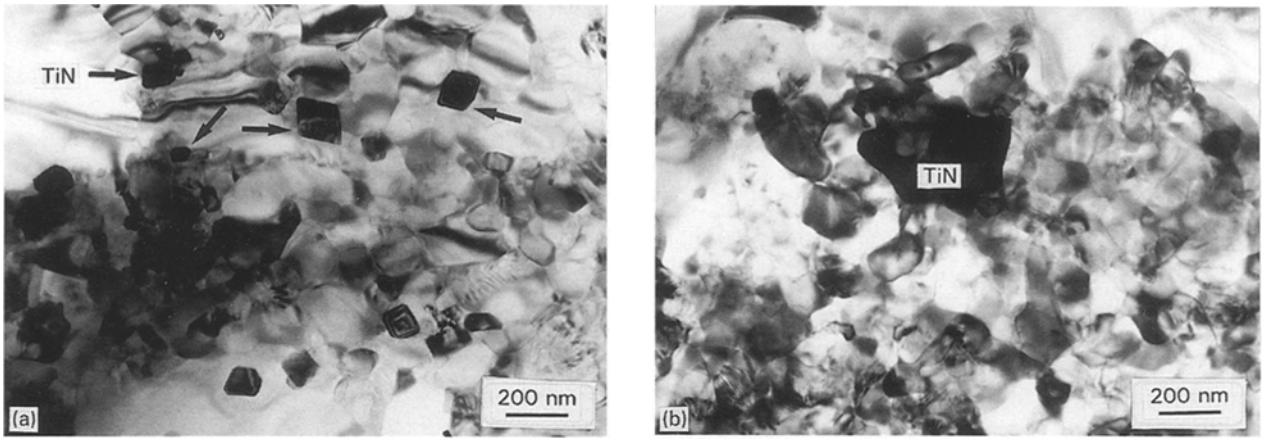

Figure 11 Transmission electron micrographs of general views of the microstructures of 1700 °C, 20 MPa and 460 s hot-pressed materials, (a) coated and (b) mixed.

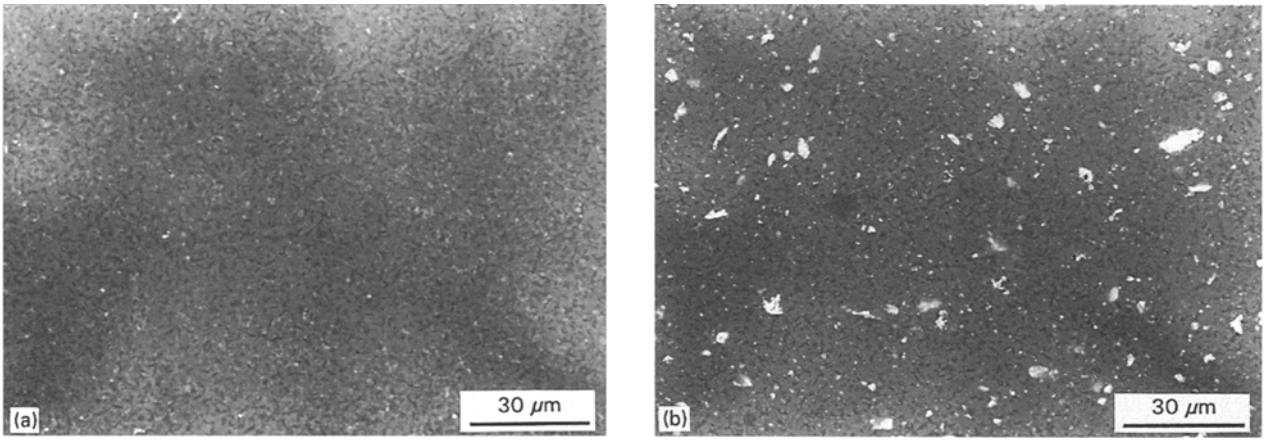

Figure 12 SEM back-scattered images in dense materials showing the distribution of TiO_2 (a) coated, and (b) mixed.

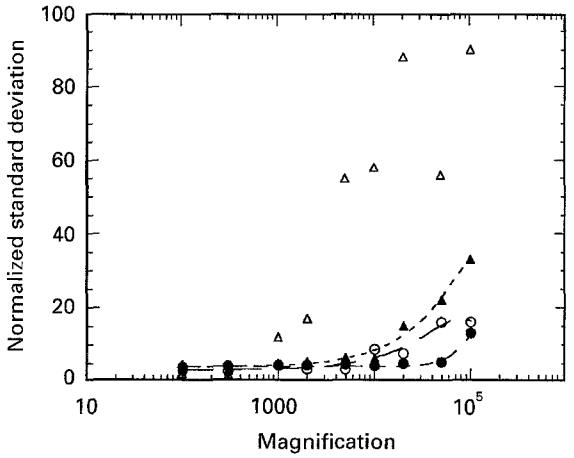

Figure 13 Normalized standard deviation of Al/(Al + Si + Ti) and Ti/(Al + Si + Ti) count ratio as a function of magnification for materials hot-pressed at 1700 °C and 20 MPa for 460 s. (▲, △) titanium, (●, ○) aluminium; (△, ○) mixed, (●, ▲) coated.

TABLE I Phase distribution homogeneity dimension for Si_3N_4 green compacts, and after hot pressing at 1700 °C and 20 MPa for 460 s

Materials		Homogeneity dimension			
		Al		Ti	
		(μm)	N^a	(μm)	N^a
Green:	mixed	20	40	120	240
	coated	6	12	7	14
Dense:	mixed	10	10	120	120
	coated	3	3	20	20

[a] N is the homogeneity dimension measured by Si_3N_4 particle number.

dimension ~3 μm and titanium-containing phase ~20 μm.

Comparing the phase distribution homogeneity dimensions in the green state with those after densification, it is seen that the homogeneity dimension of the titanium-containing phase is substantially unchanged for mixed powder material. However, for the coated powder material, the titanium-containing phase homogeneity dimension increases, an indication of a tendency of non-homogeneous distribution of the titanium-containing phase after densification. The homogeneity dimension of the aluminium-containing phase decreases by factors of two and three for coated powder material and mixed powder material. This implies that, during densification, the aluminium is re-distributed to a more homogeneous state.

4. Discussion

The advantages at the hot-pressing stage of using coated Si_3N_4 powder are confirmed by the data for density as a function of time (Fig. 4). The coated powder reaches the final recorded relative density of 0.99 in times significantly shorter than those for the milled powder.

In densification by liquid-phase sintering, the initial stage of densification is mainly the result of particle rearrangement [31], which in turn depends on the rate of liquid formation and the initial distribution of liquid [32, 33]. The fast formation and homogeneous distribution of the liquid favour rapid particle rearrangement, and correspondingly to an initial fast densification rate. In practice, the rate of liquid formation is influenced by the particle size and degree of mixing of the liquid-forming components. Fine powder particle sizes and intimate mixing of the components accelerate the formation of liquid when the system temperature reaches the eutectic. The initial distribution of the liquid formed can also affect the densification rate, as localized pockets of liquid (a consequence of non-homogeneous distribution of the liquid-forming components) can cause local fast densification, but elsewhere in the system leaves some area "dry". The concentrated liquid phase may take some time to redistribute and, as a result, an overall initial lower densification rate may be observed. At this stage, not only intimate mixing of the sintering additive components, but also their homogeneous distribution in the host particle matrix are of great importance in determining the densification rate.

Intimate mixing of the sintering additive particles with the host particles can be limited by the particle size, size distribution and the state of particle agglomeration in both additive and host powder [34]. Ideally, the most homogeneous distribution of the sintering additive particle in the host particles should correspond to a mixing state with non-agglomerated primary particles completely isolated by the host particles, and evenly distributed. In principle, the finer, and more uniform the size distribution, of the additive particles, the more likely a homogeneous distribution will be obtained. However, in reality, for most ceramic powders, the primary particles are agglomerated as a result of the van der Waals interactions, and it is observed that the finer the primary particle size, the stronger is the tendency of agglomeration [35]. At this point, the possible advantages of using fine particle powders for obtaining homogeneous mixing of sintering additive is therefore blurred by agglomeration.

In the mixed powder, the Al_2O_3 sintering additive has an average particle size of ~ 500 nm, and the TiO_2 powder has an agglomerate size of ~ 500 nm (with a primary particle size of ~ 20 nm). These are approximately the same size as the Si_3N_4 particles. The relatively coarse size of the Al_2O_3 and the agglomeration of the fine TiO_2 particles, make it very difficult to ensure thorough contact of the individual Al_2O_3 and TiO_2 particles, and likewise their homogeneous distribution in the matrix powder. Under TEM the agglomeration of the TiO_2 could be identified within the observed area (Fig. 1b). However, in the coated powder, the fine precipitated oxide particles not only ensure intimate mixing of Al_2O_3 and TiO_2, but also ensure the homogeneous distribution of the liquid-forming components, by cladding the surface of the Si_3N_4 particles. The observed faster initial densification rate in the coated powder system seems likely to be the result of a more rapid generation of liquid phase, which is also probably more homogeneously distributed in the network of Si_3N_4 particles on attainment of the eutectic temperature. This also can be evinced by the fast α- to β-phase transformation during the initial hot pressing, for both powders, hot pressed for the same period of 460 s. 74% α-Si_3N_4 phase was identified in material derived from mixed powder, compared with 68% in materials derived from coated powder; an indication that the initial reactions are faster in the coated powder.

Quantitatively, the state of homogeneity can be described by the "homogeneity dimension", the minimum dimension in which the relative concentration of the component phases is equal to that of the bulk material. The smaller this dimension, the more homogeneous the phase distribution. In principle, the homogeneity dimension depends on the relative phase content, the existing state of the second phase (such as whether it is present as an inclusion or as a continuous network such as a grain-boundary phase), and grain size and grain-size distribution.

Consider a two-phase composite, with the second phase dispersed in the matrix in the form of inclusions with a uniform size of c_{ii} and a total volume fraction v_{ii}. Assuming a perfectly homogeneous distribution as shown in Fig. 14a, a minimum dimension a_{ii} can be quantitatively defined from the relationship

$$\left(\frac{c_{ii}}{a_{ii}}\right)^3 = v_{ii} \tag{11}$$

or

$$a_{ii} = \frac{c_{ii}}{v_{ii}^{1/3}} \tag{12}$$

where a_{ii} is the minimum dimension in the structure within which the relative phase concentration should be representative of the whole material. Equation 12 quantitatively relates the phase homogeneity dimension with the phase content and inclusion size for the ideal phase distribution, with the matrix phase regarded as a continuum. However, the real situation is that the inclusion size is not exactly uniform; the inclusion distribution in the matrix is not regular (inclusion distributions are influenced by the matrix grain size and grain-size distribution). Any deviation from the above modelled distribution will sensitively increase the homogeneity dimension, as shown in Fig. 14b.

If the second phase exists as a continuous network, such as an intergranular grain-boundary phase, it is obvious that the homogeneity dimension will be determined by the grain size, grain-size distribution, and the grain-boundary thickness distribution. A fine grain size and uniform grain-size distribution tend to correspond to a low value of the homogeneity dimension.

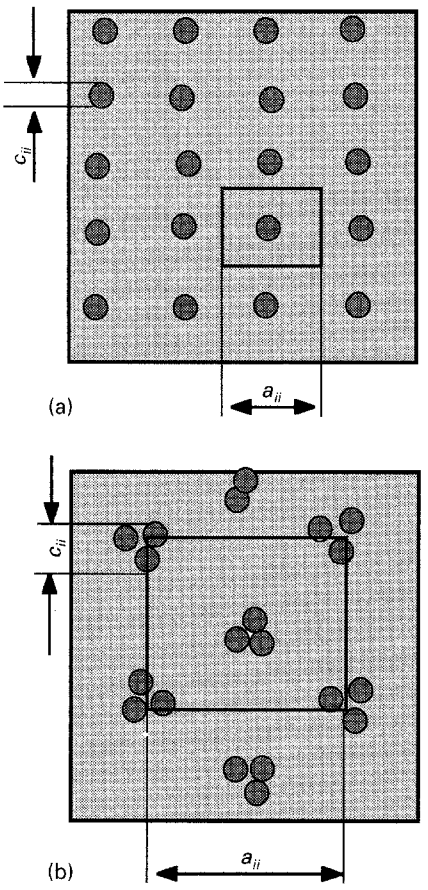

Figure 14 Homogeneity dimension changes with distribution of inclusions in the matrix.

In the mixed powder, green body homogeneity dimensions of 20 and 120 μm have been experimentally obtained for the Al_2O_3 and TiO_2-containing phases, respectively, which is far larger than the calculated values from Equation 12 (1.2 and 1.6 μm for Al_2O_3 and TiO_2 respectively, with an Al_2O_3 particle size of 500 nm and a TiO_2 agglomerate size of 500 nm). This deviation shows how far the actual distribution is from the ideal homogeneous distribution. The non-homogeneous distribution in the green compact may be inherited from a non-homogeneous mixing of the powder, or from segregation of powder during drying [36]. With the coated powder, the additive can be regarded as a continuous network between Si_3N_4 particles, and the homogeneity dimension should be about the biggest size of the Si_3N_4 particles, ~700 nm. However, the measured value is much larger, possibly as a result of coating clusters forming during coating [5].

After liquid-phase sintering, the phase distribution is changed compared with the phase distribution in the green body. For a specific phase, the change depends on the role of the phase in the sintering process. In the present case, the liquid redistribution combined with solid solution of aluminium in silicon nitride grains [37] are expected to make aluminium distributed on a fine-scale after densification; this was verified by the observed aluminium-related phase homogeneity dimension decrease after densification for both coated and mixed powders. The role of TiO_2 in the densification process involves the formation of liquid and finally conversion to TiN through the solution reprecipitation process [5]. The observed tendency of non-homogeneous distribution in the coated powder for the titanium-containing phase after densification is hence contributed to the coarsening of TiN particle size compared with initial TiO_2 particles.

The Vickers hardness and indentation fracture toughness show no substantial difference between materials processed by coating and mixed powder. In measuring these barometers, an area of about $70 \times 70\ \mu m^2$ was covered by the indent, which is around the phase distribution homogeneity size of both materials (Table I), and allows coverage of all phases present in the material. The slight decrease in hardness with increasing hot-pressing time could be the result of the changes in the relative content of α- and β-Si_3N_4 phase. It has been observed that the hardness of sintered Si_3N_4 increases with increasing α-Si_3N_4 phase content [38]; it has also been reported that the hardness of single α-Si_3N_4 crystal is higher than that of single β-Si_3N_4 crystal [36, 39–41]. The increase in fracture toughness with increasing hot-pressing time may mainly be the consequence of increased β-Si_3N_4 phase as reported [38]. However, the fracture toughness of both materials is ~ 2.5 MPa $m^{1/2}$ which is very low compared with the values of 4.0–7.0 MPa $m^{1/2}$ typical of hot-pressed Si_3N_4 [42]. This may be ascribed to the equiaxied morphology of the β′-sialon grains in this materials; the presence of high aspect ratio β′-sialon grains increases the fracture toughness by the crack deflection mechanism [42].

The Weibull modulus provides a guide for the defect-size distribution [43]. In the mixed powder material, the defect size may be bigger and have a wider distribution than that in the materials processed from coated powder. Similar results have been reported for Si_3N_4 densified with $MgAl_2O_4$ [3, 12, 44]. However, the low values for four-point bend strength in this study are possibly related to the equiaxied grain morphology. It has been established that to obtain a tough and strong Si_3N_4-based ceramic, complete α- to β-phase transformation during densification is required, and the β-Si_3N_4 grains should have high aspect ratio [45–47]. This implies that the increase in fracture toughness with hot-pressing time (Fig. 8) could derive from the α- to β-Si_3N_4 phase transformation.

5. Conclusion

Small amounts of sintering additive can be incorporated more homogeneously into a Si_3N_4 powder using a particle coating process based on alkoxide hydrolysis, compared with the standard powder mixing method.

Phase distribution homogeneity can be quantitatively described by a "homogeneity dimension", which is experimentally obtained through the use of EDS in SEM. In the green body, the mixed powder has a homogeneity dimension of ~20 μm for Al_2O_3, and of ~120 μm for TiO_2. Although the TiO_2 (~20 nm)

powder used has a smaller primary particle size than the Al_2O_3 powders ($\sim$300 nm), the significantly inhomogeneous distribution of the TiO_2 is likely to be caused by the agglomeration of TiO_2 particles. Thus on the mixing of additive powders with host powders, an additive with a very small primary particle size does not necessarily give a more homogeneous distribution. The state of agglomeration of the additive particles is an important factor in determining the degree of mixing. Compared with the mixed powders, coated powder homogeneity dimensions were smaller by a factor of 2 for Al_2O_3 and a factor of 16 for TiO_2.

On densification, the oxide additive phase is redistributed. The Al_2O_3 is redistributed on a finer scale because of the solid solution of Al_2O_3 in the β'-sialon lattice; the TiO_2 is redistributed on a coarser scale (homogeneity dimension $\sim$7 μm in the green body compared with $\sim$20 μm after densification) possibly because of the TiO_2 particle coarsening, and the conversion of TiO_2 to TiN through solution and reprecipitation process permitting some grain growth.

Coated powders densify more quickly during hot-pressing than mixed powders, and under fixed conditions can be hot-pressed to full density in a significantly shorter time ($\sim$150 s to 99% theoretical density at 1700 °C 20 MPa, compared with $\sim$250 s for mixed powder under the same hot-pressing conditions). Materials prepared using coated powders have a more homogeneous microstructure, a higher mean strength in four-point bend, and an associated higher Weibull modulus.

Acknowledgements

This work was supported partly by The Natural Science Foundation of China. C.M.W. thanks Dr F.L. Riley for his critical comments on the work.

References

1. F. F. LANGE, *J. Am. Ceram. Soc.* **72** (1989) 3.
2. F. F. LANGE and M. METCALF, *ibid.* **66** (1983) 398.
3. M. KULIG, W. OROSCHIN and P. GREIL, *J. Eur. Ceram. Soc.* **5** (1989) 209.
4. K. KISHI, S. UMEBAYASHI, R. POMPE and M. PERSSON, *J. Ceram. Soc. Jpn Int. Ed.* **96** (1988) 687.
5. C. M. WANG, PhD thesis, School of Materials, University of Leeds, Leeds, UK (1993).
6. C. L. HU and M. N. RAHAMAN, *J. Am. Ceram. Soc.* **75** (1992) 2066.
7. *Idem, ibid.* **76** (1993) 2549–54.
8. F. A. SELMI and V. R. W. AMARAKOON, *ibid.* **71** (1988) 934.
9. D. KAPOLNEK and L. C. D. JONGHE, *J. Eur. Ceram. Soc.* **7** (1991) 345.
10. Y. TAKAHASHI and J. CHIZAKI, *J. Ceram. Soc. Jpn Int. Ed.* **96** (1988) 238.
11. K. KISHI, S. UMEBAYASHI, E. TANI and K. KOBAYASHI, *Yogyo-Kyokai-Shi* **93** (1985) 629.
12. K. KISHI, S. UMEBAYASHI and K. KOBAYASHI, *ibid.* **94** (1989) 179.
13. T. M. SHAW and B. A. PETHICA, *J. Am. Ceram. Soc.* **69** (1986) 88.
14. J. S. KIM, H. SCHUBERT and G. PETZOW, *J. Eur. Ceram. Soc.* **5** (1989) 311.
15. S. BAIK and R. RAJ, *J. Am. Ceram. Soc.* **68** (1985) C124.
16. T. MAH, K. S. MAZDIYASNI and R. RUH, *Bull. Am. Ceram. Soc.* **58** (1979) 840.
17. C. M. WANG and F. L. RILEY, *J. Eur. Ceram. Soc.* **10** (1992) 83.
18. E. LIDEN, M. PERSSON, E. CARLSTROM and R. CARLSSON, *J. Am. Ceram. Soc.* **74** (1991) 1335.
19. P. F. LUCKHAM, B. VINCENT and T. F. TADROS, *Coll. Surf.* **6** (1983) 281.
20. J. C. CHANG, B. V. VELAMAKANNI, F. F. LANGE and D. S. PEARSON, *J. Am. Ceram. Soc.* **74** (1991) 2201.
21. W. J. HUPPMAN and W. BAUER, *Powder Metall.* **18** (1975) 249.
22. F. F. LANGE and M. M. HIRLINGER, *J. Mater. Sci. Lett.* **4** (1985) 1437.
23. F. F. LANGE and K. T. MILLER, *J. Am. Ceram. Soc.* **70** (1987) 896.
24. C. P. GAZZARA and D. R. MESSIER, *Bull. Am. Ceram. Soc.* **56** (1977) 777.
25. K. ICHIKAWA, in "Silicon Nitride-I," edited by S. Somiya, M. Mitomo and M. Yshimura (Elsevier Applied Science, London/New York, 1990) pp. 107–16.
26. B. BERGMAN and H. HEPING, *J. Eur. Ceram. Soc.* **6** (1990) 3.
27. T. EKSTROM, P. O. KALL, M. NYGREN and P. O. OLSSON, *J. Mater. Sci.* **24** (1989) 1853.
28. W. WEIBULL, *J. Appl. Mech.* **18** (1951) 293.
29. J. E. OVRI and T. J. DAVIES, *Sci. Ceram.* **14** (1988) 599.
30. G. R. ANSTIS, P. CHANTIKUL, B. R. LAWN and D. B. MARSHALL, *J. Am. Ceram. Soc.* **64** (1981) 533.
31. W. D. KINGERY, *J. Appl. Phys.* **30** (1959) 301.
32. R. M. GERMAN, in "Liquid Phase Sintering" (Plenum Press, London/New York, 1985) pp. 127–55.
33. C. M. WANG, *J. Mater. Sci.* **30** (1995) 3222.
34. R. HOGG, *Bull. Am. Ceram. Soc.* **60** (1981) 206.
35. K. KENDALL, N. M. ALFORD, W. J. LEGG and J. D. BIRCHALL, *Nature* **339** (1989) 11.
36. G. E. GAZZA, p. 273 in Progress in Nitrogen Ceramics, Ed. F. L. Riley, Martinus Nijhoff, 1983.
37. D. A. BONNEL, M. RUHLE and T. Y. TIEN, *J. Am. Ceram. Soc.* **69** (1986) 623.
38. E. M. K. WEDEL, L. K. L. FALK, H. BJORKLUND and T. EKSTROM, *J. Mater. Sci.* **26** (1991) 5575.
39. G. R. TERWILLIGER and F. F. LANGE, *J. Am. Ceram. Soc.* **57** (1974) 25.
40. C. GRESKOVICH and H. C. YEH, *J. Mater. Sci. Lett.* **2** (1985) 657.
41. C. GRESKOVICH and G. E. GAZZA, *ibid.* **4** (1987) 195.
42. G. ZIEGLER, J. HEINRICH and G. WOTTING, *J. Mater. Sci.* **22** (1987) 3041.
43. K. TRUSTRUM, *ibid.* **14** (1979) 1080.
44. S. SIEGEL, M. HERRMANN, H. KLEMM and S. KEBLER, in "Proceedings of the Second European Ceramic Conference", Augsburg, FRG (1991).
45. F. F. LANGE, *Int. Met. Rev.* **247** (1980) 1.
46. F. F. LANGE, *Bull. Am. Ceram. Soc.* **62** (1987) 1369.
47. T. EKSTROM, L. K. L. FALK and E. M. K. WEDEL, *J. Mater. Sci.* **26** (1991) 4331.

Received 11 April 1994
and accepted 13 February 1996